Available online at www.sciencedirect.com
SCIENCE DIRECT®
Earth and Planetary Science Letters 244 (2006) 201–217
EPSL
www.elsevier.com/locate/epsl

Discovery of whitlockite in mantle xenoliths: Inferences for water- and halogen-poor fluids and trace element residence in the terrestrial upper mantle

Dmitri A. Ionov [a,b,*], Albrecht W. Hofmann [a], Claude Merlet [c], Andrey A. Gurenko [a], Eric Hellebrand [a], Gilles Montagnac [d], Philippe Gillet [d], Vladimir S. Prikhodko [e]

[a] *Max-Planck-Institut für Chemie, Postfach 3060, D-55020 Mainz, Germany*
[b] *Institut für Mineralogie, J.W. Goethe-Universitaet, Senckenberganlage 28, 60054 Frankfurt/Main, Germany*
[c] *Laboratoire de Tectonophysique (UMR 5568 CNRS), Université Montpellier 2, 34095 Montpellier, France*
[d] *Laboratoire de Sciences de la Terre, Ecole Normale Supérieure de Lyon, 46 allèe d'Italie, 69364 Lyon, France*
[e] *ITIG, Russian Academy of Sciences, 680063 Khabarovsk, Russia*

Received 24 November 2005; received in revised form 7 February 2006; accepted 7 February 2006
Available online 13 March 2006
Editor: R.W. Carlson

Abstract

Chemical analyses and Raman micro-spectroscopy have identified whitlockite (water- and halogen-free phosphate) in mantle xenoliths from Siberia. Whitlockite has not previously been reported from terrestrial mantle-derived rocks, but is the most common accessory phosphate in meteorites and igneous rocks from Mars and the Moon. The presence of the 'anhydrous' whitlockite, together with the breakdown of 'hydrous' accessory minerals (amphibole, phlogopite) in the same xenoliths, indicates that portions of the terrestrial upper mantle may be nearly as low in water and halogens as in inner parts of the smaller solar system bodies, regardless of enrichments of other highly mobile components (phosphorus, alkalis). Whitlockite may be an important host for some lithophile trace elements in those portions of the terrestrial mantle. It contains up to 3 times more rare earth elements than coexisting apatite but less Sr, Ba and U while Th abundances are similar. Thus, trace element abundances, patterns and ratios (e.g. Sr/Nd, Th/U) in whitlockite-bearing mantle rocks and coexisting fluids may be distinct from those for mantle rocks containing only apatite and/or other 'hydrous' minerals. Several generations of both whitlockite and apatite with different textural positions and abundances of Na, Mg, Sr and LREE were identified in some of the xenoliths. Furthermore, precipitation of the phosphates was accompanied by the formation of a distinct generation of clinopyroxene, which contains much less Zr (up to 10 times) but more LREE than clinopyroxenes formed in previous metasomatic episodes.

Keywords: whitlockite; apatite; terrestrial mantle; metasomatism; trace elements; volatiles

1. Introduction

There is no doubt that water plays a fundamental role in the formation and evolution of terrestrial continents and oceans, and it is widely believed that water is also an essential prerequisite for the development of plate

* Corresponding author. Institut für Mineralogie, J.W. Goethe-Universitaet, Senckenberganlage 28, 60054 Frankfurt/Main, Germany. Tel./fax: +49 6131 305281.
E-mail address: ionov@mpch-mainz.mpg.de (D.A. Ionov).

0012-821X/$ - see front matter © 2006 Elsevier B.V. All rights reserved.
doi:10.1016/j.epsl.2006.02.012

tectonics [1]. Until fairly recently, it was thought that the Earth's deeper interior is essentially dry because dehydration reactions during subduction liberate the water and because hydrous phases were considered to be unstable at depths below about 100 km [2–4]. In recent years, however, experimental studies have shown that at very high pressures, nominally 'anhydrous' silicate minerals can accommodate substantial amounts of water [5]. Moreover, the post-olivine high-pressure phases ringwoodite and wadsleyite appear to have solubilities of water in the percent range [6]. This has led to speculations that a "whole ocean" might be buried in the deep mantle, all dissolved in common silicate minerals, as in the widely discussed "water filter" hypothesis of Bercovici and Karato [7].

This reignites the discussion of what the actual water content of the mantle might be. The presence of 'hydrous' phases (such as phlogopite, amphibole and apatite) in 'metasomatic' assemblages found in many mantle xenoliths (e.g. [8–10]) lends some support to the notion that water is ubiquitous in the mantle. This is in sharp contrast with the mineralogy of lunar rocks, chondritic and iron meteorites, and Martian meteorites, which are dominated by 'dry' assemblages. This contrast is highlighted by the common presence of the anhydrous and halogen-free phosphate mineral whitlockite $(Ca,Mg)_3[PO_4]_2$ in lunar and meteoritic rocks [11–16], whereas in terrestrial mantle rocks, phosphates have been thought to occur exclusively in their hydrous form, apatite $Ca_5[PO_4]_3[OH,F,Cl]$ ([9,10], references therein). On Earth, whitlockite occurs mainly in pegmatites (type locality is the Palermo mines, New Hampshire, USA), sedimentary rocks and biomaterials. Here we report the first find of whitlockite in terrestrial mantle xenoliths [17]. This raises the question whether some of the phosphates in mantle rocks, which are routinely identified as 'apatite', might actually be whitlockite. It further indicates that water may be far from ubiquitous in the lithospheric mantle and that unknown, but possibly quite significant portions of terrestrial mantle are essentially dry and poor in halogens in spite of being metasomatically enriched in highly incompatible elements.

Apatite is one of the most important accessory hosts of incompatible elements in mafic and ultramafic rocks. Earlier xenolith studies have indicated that significant proportions of Th, U and light rare earth elements (LREE) in the terrestrial upper mantle can be hosted by apatite ([9,10], references therein). We show that abundances of many trace elements in coexisting whitlockite and apatite are different, in particular whitlockite has higher REE contents and lower Sr/Nd and U/Th. Thus, element abundances in whitlockite and apatite in equilibrium with the same fluid should be different and hence the identity of accessory phosphate species may affect trace element signatures of both mantle rocks and percolating fluids.

2. Samples and methods

Whitlockite was found in fragments of upper mantle peridotites (spinel harzburgites and lherzolites equilibrated at 890–950 °C) hosted by Quaternary alkali basaltic lavas at Tok in the southeastern Siberian craton, Russia [18]. Detailed information about petrography, chemical and isotope composition of the xenoliths and their major minerals has been given in [18–21]. Ionov et al. [19] provide a brief description of phosphates in some Tok xenoliths and suggest that they may be important hosts of LREE in bulk rocks. The main goal of this paper is to consider in detail mineralogy, chemical composition and the origin of whitlockite, apatite and associated accessory phases and to explore the geochemical role of whitlockite in the continental lithospheric mantle (CLM) beneath Tok and in the terrestrial upper mantle in general; these topics were not considered in previous publications on Tok xenoliths.

Whitlockite, apatite and coexisting phases were identified using Raman micro-spectroscopy at Laboratoire de Sciences de la Terre, ENS-Lyon [22]. Raman scattering was excited using a He–Ne laser beam at $\lambda = 632.8$ nm (1.96 eV) and power <2.5 mW. Unpolarised Raman spectra were acquired with a Labram HR800 model of Jobin-Yvon Horiba spectrometer equipped with a microscope for collection of back-scattered Raman signals. Spectral resolution was about 4 cm^{-1}.

Chemical compositions of minerals were obtained by electron probe micro-beam analysis (EPMA) on two instruments. One is a Jeol Superprobe JXA-8200 at the Max-Planck-Institut für Chemie in Mainz. Phosphates, mica and feldspar were analysed using 15 kV accelerating voltage, 12 nA primary beam current and 1–8 μm beam size; olivine, spinel and oxides were analyzed using 20 kV, 20 nA and a focussed beam; counting times were 30–60 s on peaks and 15–30 s on background. Reference materials from the Smithsonian Institution [23] and Micro-Analysis Consultants Ltd (UK) were used for calibration. Element mapping was done using 15 kV voltage and 12 nA beam current in stage scanning mode registering simultaneously X-ray signals of five wavelength dispersive spectrometers and back-scattered electron (BSE) images. The step interval was 1 μm, measurement time per step (dwell-time) was 300 ms.

LREE in phosphates were determined on a CAMECA SX-100 instrument at Service Microsonde Sud (Université Montpellier 2) using techniques described in [19].

Trace element abundances in phosphates and clinopyroxenes (cpx) were determined by secondary ion mass-spectrometry (SIMS) on an upgraded Cameca 3f instrument in Mainz using established techniques [24]. ^{44}Ca was used as a reference mass. Sensitivity factors were defined on homogeneous chips of the Durango apatite previously analysed in Mainz by LA-ICPMS using NIST-612 reference glass as external standard [19].

3. Results

3.1. Petrographic and Raman micro-spectroscopy data

Whitlockite occurs as small (<100 μm), mainly anhedral grains in interstitial pockets and veins, commonly in association with alkali feldspar and fine-grained, 2nd-generation olivine, spinel and cpx (Fig. 1a). Less commonly, whitlockite mantles massive apatite (Fig. 1e) or forms vermicular intergrowths with feldspar (Fig. 2a). Whitlockite may coexist with apatite (Fig. 1b–d); in some cases the two minerals are intergrown (Fig. 1c) or form spongy mosaic

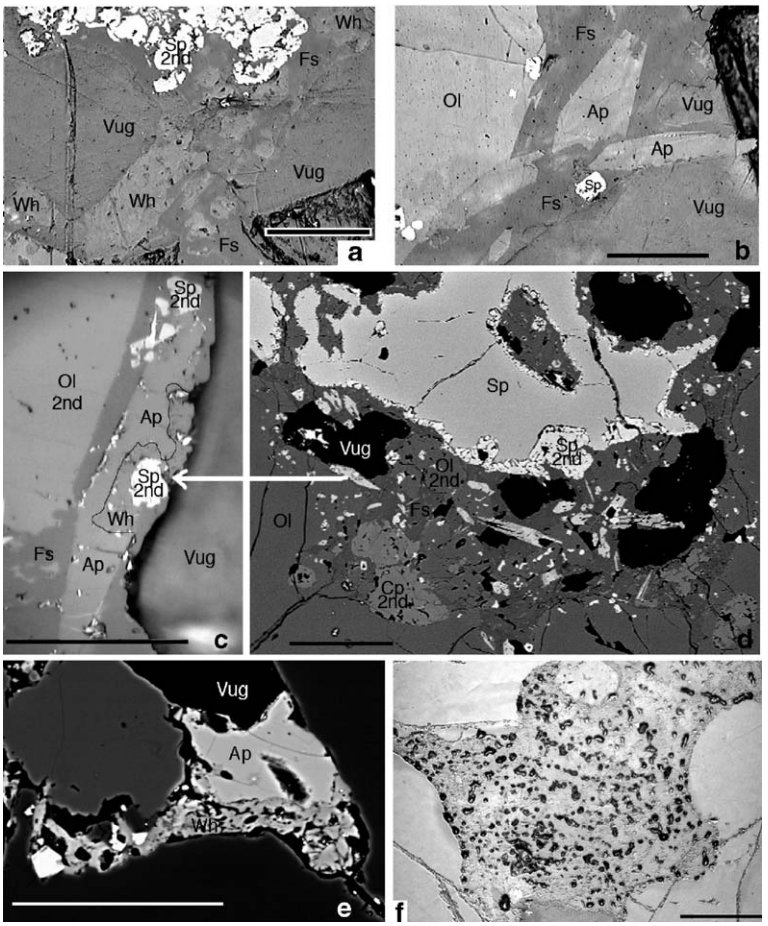

Fig. 1. (a–d) Whitlockite (Wh) and apatite (Ap) in peridotite xenolith 5-3 from Tok. The phosphates occur in fine-grained metasomatic aggregates together with second-generation olivine (Ol), clinopyroxene (Cp) and spinel (Sp) in alkali-feldspar (Fs) matrix with abundant vugs. (a–c) Photomicrographs in reflected light: (a) anhedral whitlockite, (b) prismatic apatite, (c) composite apatite–whitlockite grain. Scale bars, 60 μm. A black line is drawn along the Wh–Ap boundary in (c) because the two minerals (identified by Raman micro-spectrometry and EPMA) are hard to distinguish optically. Black areas in (a) and (b) are pits burned by electron beam scans in epoxy resin filling vugs. (d) Back-scattered electron (BSE) image of a phosphate-bearing aggregate. Note that primary Sp and Ol have rims of 2nd-generation Sp and Ol when in contact with the Fs-bearing aggregates and hence are not in equilibrium with those metasomatic assemblages. White arrow indicates the Wh–Ap grain shown in detail in (c). Scale bar, 200 μm. (e) BSE image of massive interstitial apatite partially rimmed with spongy whitlockite in sample 8-31. Scale bar, 100 μm. (f) Spongy apatite aggregate in xenolith 1-1 (reflected light). Scale bar, 100 μm.

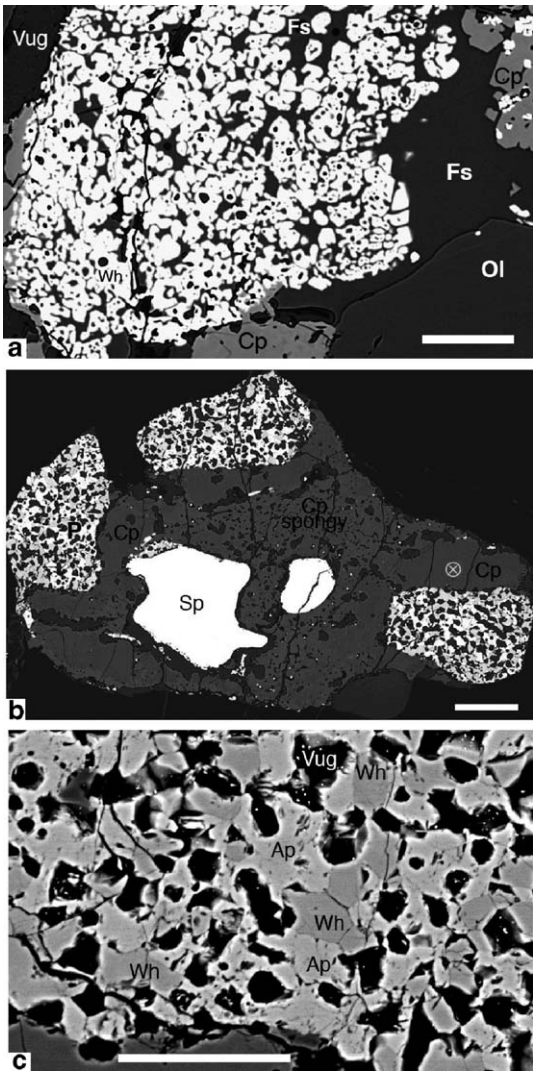

Fig. 2. BSE images of spongy and vermicular phosphates in Tok peridotite xenolith 8-40. Abbreviations are as in Fig. 1. (a) Vermicular whitlockite (white) intergrown with alkali feldspar. Scale bar, 50 μm. (b) Spongy Wh–Ap aggregates intergrown with normal (not late-stage, spongy) Cp. White circled cross shows the Cp spot analysed by SIMS (Table 3). Scale bar, 100 μm. (c) Details of the spongy Wh–Ap aggregate. Empty cavities initially contained fluid, which may have escaped shortly before or during the transport from the mantle. The xenolith does not contain 'hydrous' silicate phases and hence the hypothetical fluid is inferred to have been poor in water and consisted mainly of dense CO_2 or liquid carbonates because hydrous fluids react with wall-rocks to produce amphibole or phlogopite (see also Fig. 1d–f). Scale bar, 50 μm. Very similar spongy Wh–Ap aggregates occur in xenolith 6-0.

aggregates (Fig. 2b, c) and appear to be in textural equilibrium. The metasomatic aggregates, which contain whitlockite, commonly have empty cavities ('vugs'; Figs. 1 and 2); whitlockite also occurs on the walls or inside bigger cavities (Fig. 1d, bottom right).

Whitlockite is slightly darker than apatite in reflected light (Fig. 1c) and in BSE images (Figs. 1e and 2c); unlike apatite, whitlockite does not normally form euhedral grains (cf. Fig. 1a and b). In general, however, whitlockite and apatite look very similar under microscope and on BSE images; they were identified in most of the Tok xenoliths in this study by Raman microspectroscopy. Twin peaks at 959 and 975 cm^{-1} are characteristic of whitlockite Raman spectra whereas apatite yields a single peak at 961 cm^{-1} (Fig. 3a).

Accessory amphibole and phlogopite occur in some Tok xenoliths including those containing apatite [18,20]. Many other apatite-bearing mantle peridotites worldwide contain amphibole and/or phlogopite as well

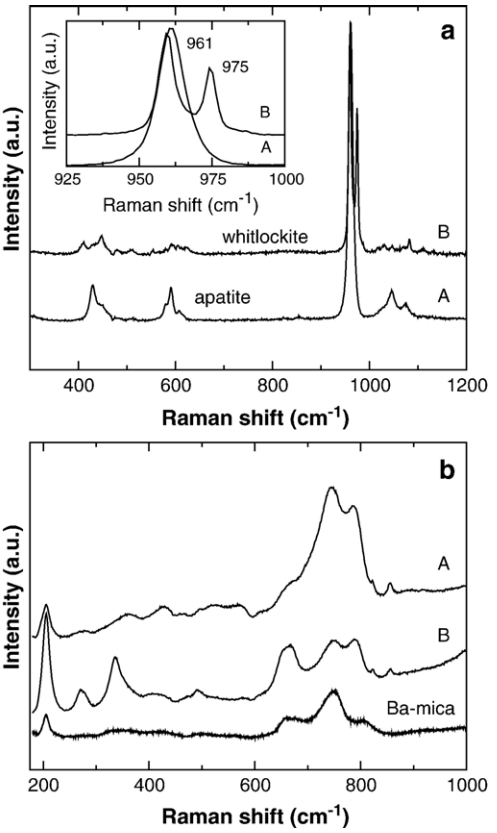

Fig. 3. Raman spectra of minerals in Tok xenoliths. (a) Apatite and whitlockite in sample 5-3 (Fig. 1a–d). Raman peak intensities between 925 and 1000 cm^{-1} (inset) correspond to the stretching vibration of $(PO_4)^{3-}$ tetrahedra. A single peak at 961 cm^{-1} is characteristic of apatite (spectrum A) whereas peaks at 959 and 975 cm^{-1} are indicative of whitlockite (spectrum B). (b) Ba–Ti-rich silicate in sample 8-40: spectrum A is for a prismatic grain section (Fig. 4b and d right); spectrum B is for a hexagonal grain section (Fig. 4d left). Positions of individual peaks in both spectra are similar to those for a Ba-rich mica from Pamir [35] (at bottom, see text), indicating that the Ba–Ti-rich silicate from Tok is likely a mica. Minor peaks in spectra A and B at ~850 cm^{-1} are due to olivine micro-inclusions.

[8,9,25–29]; apatite in such rocks is usually texturally equilibrated with these 'hydrous' alkali-rich minerals (Fig. 4a). By contrast, no unaltered amphibole or phlogopite has been found in any whitlockite-bearing Tok xenoliths. Some of the latter, however, contain fine-grained aggregates of elongated, sub-parallel grains of secondary olivine, spinel and Ti-rich minerals in alkali-feldspar matrix (Fig. 4b). Very rarely, such aggregates enclose resorbed relics of mica or amphibole (Table 1) and hence are breakdown products of those 'hydrous' minerals [19]. Moreover, such aggregates usually preserve the shapes and cleavage cracks of the pre-existing minerals, with the elongated olivine grains parallel to the pre-existing cleavage (cf. Fig. 4b and c). Raman spectra of the feldspar are similar to those of sanidine. No silicate glass was found in association with whitlockite or decayed 'hydrous' minerals based on petrographic, Raman and EPMA data.

The most common Ti-rich phases in the breakdown products of phlogopite and amphibole in Tok xenoliths are Fe–Ti oxides (ilmenite and armalcolite; Table 1, [18,19]). In this regard, they are similar to alkali–feldspar-bearing xenoliths earlier reported from southern and SE Siberia [30–32] as well as other localities [31,33,34]. By contrast, the breakdown products of the 'hydrous' minerals in some whitlockite-bearing Tok xenoliths contain an unusual Ba–Ti-rich (see next section) silicate phase [17], which to the best of our knowledge has not been previously reported from mantle rocks elsewhere. The Ba–Ti-rich silicate forms small ($\leq 15\,\mu m$) crystals with cross-sections ranging from hexagonal to prismatic (Fig. 4b, d). The shapes of the Raman spectra of the Ba–Ti-rich silicate in the hexagonal and prismatic sections are somewhat different, but both contain the same characteristic peaks, which were also detected for Ba-rich mica in a pyroxenite xenolith from Pamir [35] (Fig. 3b; Table 1) used in this study for comparison. Based on the morphologic and Raman spectra evidence, the Ba–Ti-rich silicate in the Tok xenoliths is most likely a mica variety [22,36].

We have found no co-existing phlogopite and Ba–Ti-rich silicates in the Tok xenoliths (and hence no direct micro-structural evidence for the inferred derivation of the latter from the former). On the other hand, a search for similar features in 'hydrous' peridotite xenoliths from central and NE Asia has shown that some phlogopites in xenoliths from Tariat in Mongolia [9,37,38] are rimmed with fine-grained materials containing alkali feldspar, olivine and a Ba–Ti-rich silicate (Fig. 4c; Table 1; Electronic Supplement), like the late-stage aggregates in the Tok peridotites. It is likely that those features in the

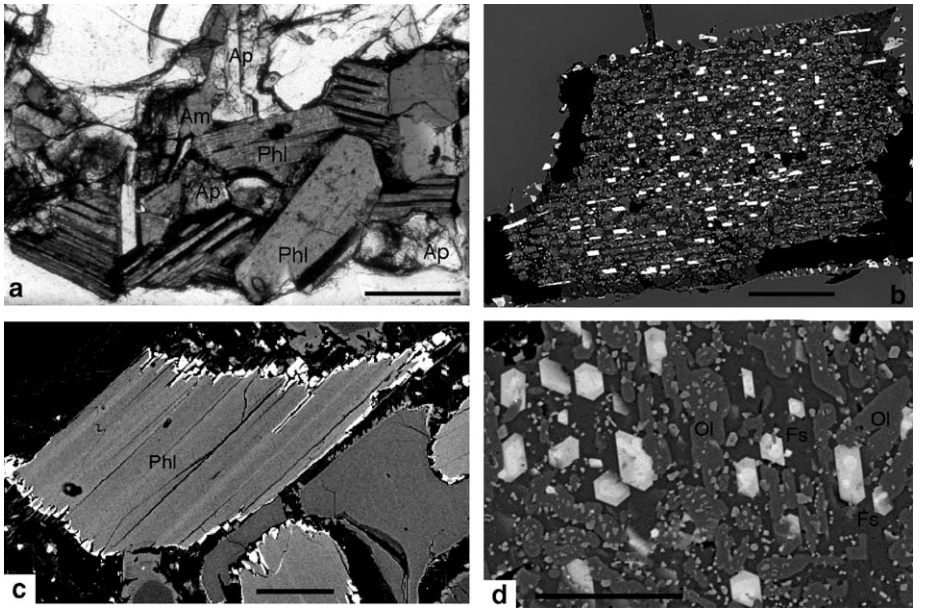

Fig. 4. (a) Photomicrograph of a phlogopite–amphibole–apatite (Phl–Am–Ap) vein in peridotite xenolith 8601-17 from Bartoy, southern Baikal region [9]. Note that apatite is texturally equilibrated with the other 'hydrous' minerals. Scale bar, 500 μm. (b–d) BSE images of mica breakdown products in mantle peridotite xenoliths. (b) Mica (?) grain completely replaced by aggregates of elongated Ol (grey) and prismatic Ba–Ti-rich silicate (white), both parallel to the cleavage of the pre-existing mica, set in an alkali-Fs matrix. Sample 8-40 from Tok; scale bar, 100 μm. (c) Phl grain replaced at rims by an aggregate of Ba–Ti-rich silicate, alkali-Fs and Ol (Table 2). Sample 8530-26, Tariat, Mongolia; scale bar, 100 μm. (d) Different cross-sections of the Ba–Ti-rich silicate crystals (light grey) range in shape from prismatic to hexagonal. Their cores are lighter than rims because of higher Ba (Table 2). Sample 8-40; scale bar, 50 μm.

Table 1
EPMA of phlogopite and its breakdown products

Sa. type	Tok phlogopites				Tok Ba–Ti-micas						
Sa. no.	1–14	3–28	3–29	10–26	8-1	8-40 (Fig. 4d)					Pamir
Mineral	Phl	Phl	Phl	Phl		Core 1	Core 2	Rim	Cr-rich		Ba–Phl
Notes	Av. 2	Av. 3	Av. 2	Av. 2	Av. 6	Av. 3	Av. 3	Av. 5	Euhedr.	Poikil.	Av. 4
SiO_2	37.39	36.02	37.69	37.48	31.89	26.64	28.18	30.71	30.77	35.44	29.16
TiO_2	2.23	3.33	2.74	6.08	15.34	15.15	15.65	15.45	8.04	0.76	5.41
Al_2O_3	16.85	17.10	17.11	15.66	16.22	17.82	17.90	16.80	18.84	31.52	17.14
Cr_2O_3	1.96	1.72	1.45	1.10	1.45	1.34	1.18	1.43	5.91	8.38	0.02
FeO	4.02	3.92	3.85	6.15	5.02	4.48	4.69	4.63	4.42	3.85	2.19
MnO	0.01	0.02	0.01	0.04	0.04	0.00	0.04	0.01	0.06	0.06	0.06
MgO	21.59	20.96	21.85	18.90	13.42	12.10	12.72	13.05	13.41	7.95	20.49
CaO	0.00	0.01	0.01	0.00	0.05	0.03	0.01	0.03	0.11	0.43	0.00
Na_2O	0.84	0.84	0.82	0.91	0.88	0.78	0.91	0.94	1.02	2.11	0.08
K_2O	8.95	8.26	8.81	8.62	5.90	3.04	3.36	4.88	4.02	3.58	3.64
BaO	1.59	3.75	1.70	0.39	8.90	17.30	14.85	10.09	7.80	6.79	18.21
Cl	0.09	0.08	0.03	0.03	0.01	n.d.	0.02	0.05	n.d.	n.d.	0.01
F	0.16	0.16	0.29	0.29	0.17	n.d.	0.01	0.00	n.d.	n.d.	2.08
Total	95.81	96.29	96.48	95.83	99.44	98.66	99.68	98.43	94.46	100.93	98.55
Mg#	0.905	0.905	0.910	0.85	0.83	0.83	0.83	0.83	0.84	0.79	0.94

Sa. type	Composite mica (Fig. 4c)				Phl breakdown products					Fs at whitlockite	
Sa. no.	8530-26 (Tariat, Mongolia)				Tok 8-3			Tok 8-40 (Fig. 4d)		Tok 8-40	
Mineral	Phl	Ba–Ti-mi	Ol	Fs	Phl relic	Armalc.	Fs	Ol*	Spl	Fs	Fig. 2a
Notes	Av. 3	Av. 6			Av. 2		Av. 2	Av. 6	Av. 2	8 μm	Av. 2
SiO_2	37.16	33.86	41.26	63.65	39.07	0.16	59.69	41.26	1.82	60.13	61.10
TiO_2	4.66	9.87	0.05	1.14	4.17	69.55	0.51	n.d.	0.79	0.30	0.76
Al_2O_3	16.23	17.08	0.04	19.87	16.11	2.42	24.67	0.35	52.91	26.52	23.68
Cr_2O_3	0.65	1.03	0.02	0.02	1.91	1.47	0.08	0.23	14.26	0.12	0.00
FeO	3.72	4.33	8.57	0.92	2.35	8.77	0.31	7.03	8.75	0.29	0.58
MnO	0.04	0.03	0.10	0.03	0.02	0.11	0.03	0.10	0.10	0.00	0.02
MgO	21.54	16.84	50.37	0.24	20.57	12.98	0.15	50.49	21.07	0.13	0.41
CaO	0.02	0.17	0.09	3.24	0.06	0.01	0.43	0.12	0.03	0.13	0.34
Na_2O	0.85	0.99	0.01	3.55	0.99	0.00	6.93	n.d.	n.d.	11.71	6.11
K_2O	8.03	6.06	0.00	5.01	8.52	0.09	6.50	n.d.	n.d.	0.20	5.77
BaO	2.81	7.45	0.04	0.13	0.37	0.73	0.02	n.d.	n.d.	0.05	0.33
Cl	0.02	0.01	0.00	0.08	0.02	0.00	0.02	n.d.	n.d.	n.d.	0.09
F	0.75	1.40	0.00	0.06	n.d.	n.d.	n.d.	n.d.	n.d.	n.d.	0.02
Total	96.58	99.27	100.69	98.27	94.19	96.29	99.44	99.91	99.72	99.59	99.69
Mg#	0.912	0.87	0.913		0.94	0.73		0.93	0.81		

Phl, phlogopite; Ol, olivine; Spl, spinel; Fs, feldspar; Mi, mica; Armalc., armalcolite; n.d., not determined. Ol*, contains 0.33% NiO.
Ol, Spl and armalcolite are fine-grained secondary minerals in breakdown products of mica and amphibole.

Tariat xenoliths reveal early stages of the same 'dehydration' process that caused the complete breakdown of phlogopite in the Tok xenoliths.

3.2. Major element compositions of accessory phases

In addition to optical microscopy, we looked for accessory phosphates in several P-rich ($\geq 0.06\%$ P_2O_5) Tok xenoliths using EPMA element mapping (1–4 polished sections per sample) in stage scanning mode with 1 μm steps registering signals for P and BSE images (see also [19]). The scanning data confirmed that the phosphates are irregularly distributed and occur mainly as networks or clusters at certain (but not all) grain boundaries and fine-grained pockets. The phosphates were studied by EPMA using techniques optimised for specific groups of major and trace elements (Tables 2 and 3; Electronic Supplement).

Table 2 lists contents of major oxides, BaO, SrO, Cl and F in whitlockite and apatite in four xenoliths from Tok as well as for apatite in six peridotite xenoliths from southern Siberia and Mongolia. Phosphate generations with distinct compositions exist in some Tok xenoliths; major oxide variations within each generation are usually

Table 2
EPMA of phosphates in mantle peridotite xenoliths

Whitlockite and apatite in Tok xenoliths								
Sa. no.	1-1	5-3		8-40			10-19	
Miner.	Ap	Wh	Ap	Wh-ver	Wh	Ap	Wh	Ap
No. anal.	Av. 7	Av. 3	Av. 9	Av. 4	Av. 13	Av. 9		Av. 19
SiO_2	0.43	0.33	0.59	0.39	0.27	0.54	0.75	0.53
FeO	0.24	0.32	0.29	0.27	0.30	0.19	0.46	0.32
MgO	0.31	3.50	0.36	3.52	3.48	0.35	3.51	0.47
CaO	51.4	46.1	52.9	44.0	44.7	51.6	44.3	51.1
Na_2O	0.38	2.96	0.58	2.82	2.92	0.54	2.32	0.60
K_2O	0.03	0.11	0.02	0.17	0.09	0.01	0.10	0.01
P_2O_5	41.8	46.2	42.0	47.0	46.5	42.5	45.0	41.2
BaO	0.02	0.03	0.02	0.03	0.04	0.04	0.02	0.02
SrO	2.96	0.18	0.42	1.99	1.47	2.23	1.40	2.01
Cl	2.72	0.01	1.21	0.00	0.00	1.72	0.00	0.63
F	0.52	0.01	1.46	0.00	0.00	1.51	0.02	1.97
Total	100.1	99.8	99.1	100.3	99.9	100.4	98.1	98.0
Mg#	0.69	0.95	0.69	0.96	0.95	0.76	0.93	0.72

Apatite in mantle xenoliths from southern Siberia and Mongolia								
Sa. no.	621-36	604-15		Mo-96	Sv-32	9419-5	9429-20*	
Notes		Spongy aggregates					Spongy	Massive
No. anal.				Av. 3	Av. 3	Av. 3	Av. 4	Av. 4
SiO_2	0.47	0.23	0.23	0.58	1.00	0.49	0.24	1.31
FeO	0.28	0.38	0.66	0.45	0.50	0.29	0.35	0.22
MgO	0.30	0.62	3.10	1.09	0.03	0.55	0.90	0.79
CaO	51.4	53.1	48.9	51.6	53.9	49.4	50.5	52.4
Na_2O	0.36	0.05	1.06	0.75	0.08	1.02	1.29	0.67
K_2O	0.00	0.06	0.06	0.02	0.09	0.00	n.d.	n.d.
P_2O_5	43.5	42.5	42.1	41.2	43.0	41.9	37.9	36.9
BaO	0.00	0.00	0.07	0.03	0.03	0.01	n.d.	n.d.
SrO	2.43	0.77	0.65	0.38	0.92	2.37	2.18	1.26
Cl	1.88	1.38	0.17	0.26	3.60	0.15	2.07	1.20
F	2.36	0.48	3.09	1.24	0.69	1.55	0.48	0.61
Total	101.6	99.1	98.8	97.1	103.0	97.1	95.9	95.3
Mg#	0.66	0.75	0.89	0.81		0.77	0.82	0.87

Ap, apatite; Wh, whitlockite; Wh-ver, vermicular whitlockite (Fig. 2a). Totals are corrected for Cl, F^-. Sample origin: 604-15, Hamar-Daban, 621-36, Vitim, Baikal region; Sv-32, Sveyaga, Russian far east; 9419-5, 9429-20, SE Mongolia; Mo-96, central Mongolia. *Analysed with a Jeol JXA-8900 at Institut für Mineralogie, Goethe-Universitaet, Frankfurt/Main, Germany.

narrow. For example, massive interstitial whitlockite in samples 8-31 (Fig. 1e) and 10-19 has less Na_2O (0.75–1.8%; Table 3) than whitlockite in fine-grained pockets (2.3–3.0% Na_2O). In general, the contents of MgO (3.3–3.7%) and Na_2O in whitlockite are much higher than in coexisting apatite (≤1%; Fig. 5). Whitlockite also has more FeO, K_2O and P_2O_5, less CaO and SrO, and higher Mg# than coexisting apatite. Importantly, the abundances of Cl and F in the whitlockite are below EPMA detection limits (0.02–0.1%) whereas coexisting apatite has variable but generally high F and Cl contents (0.5–3%). These chemical differences are typical and persist even if the two minerals are intergrown on a μm-scale as shown by mineral mapping of their complex aggregates (Electronic Supplement). Abundances of BaO in both phosphates (Table 2) are close to EPMA detection limits (≤0.04%, e.g. they do not exceed those obtained for olivine, Table 1).

The composition of apatite in the Tok xenoliths falls within the range for apatite from other mantle peridotites in Tables 2 and 3 or reported in the literature [9,25–27,39]. Broad in-sample Na and Mg variations were found in some apatites in this study (Tables 2 and 3), yet their Na and Mg contents remain below those typical of the Tok whitlockite. Similarly, the Cl and F abundances in the apatite vary broadly but are usually complementary and remain well above the detection limits.

Table 3
LREE, Sr and halogens in phosphates from mantle xenoliths determined by EPMA (wt.%)

Sa. no.	Durango apatite (reference)				Tok 8-31						Tok 8-40 (Fig. 2c)				Tok 1-2
Mineral	Ap		Recom. Values	LA	Wh		Wh2 Fig. 1e	Ap		Ap2 Fig. 1e	Wh		Ap		Ap
No. anal.	Av. 3	1σ		Av. 6	Av. 3	1σ		Av. 6	1σ		Av. 3	1σ	Av. 4	1σ	
MgO	b.d.		0.01	n.d.	3.34	0.10	3.68	0.33	0.11	0.96	3.43	0.02	0.17	0.01	0.10
CaO	54.11	0.14	54.02	54.0	45.02	0.33	46.39	53.14	0.44	50.37	45.20	0.31	51.61	0.16	53.23
Na_2O	b.d.		0.23	n.d.	2.82	0.05	0.75	0.04	0.04	0.68	2.52	0.04	0.14	0.03	0.00
P_2O_5	42.46	0.18	40.78	n.d.	46.47	0.24	44.34	42.62	0.35	41.40	47.04	0.19	42.42	0.11	41.99
Cl	0.42	0.01	0.41	n.d.	0.01	0.01	0.02	0.50	0.10	0.68	0.01	0.01	2.51	0.07	0.22
SrO	0.03	0.00	0.07	0.05	0.85	0.30	1.83	1.21	0.31	2.08	1.52	0.04	2.78	0.04	0.79
La_2O_3	0.40	0.01	0.49	0.35	0.29	0.06	0.25	0.18	0.02	0.22	0.21	0.02	0.09	0.01	0.30
Ce_2O_3	0.48	0.01	0.55	0.43	0.57	0.09	0.46	0.34	0.03	0.43	0.46	0.01	0.18	0.02	0.44
Nd_2O_3	0.14	0.01	0.23	0.11	0.26	0.03	0.19	0.14	0.07	0.16	0.21	0.01	0.07	0.01	0.16
Total*	98.0	0.3	96.8		99.6	0.4	97.9	98.5	0.7	97.0	100.6	0.3	100.0	0.2	97.1
$(La/Nd)_{PM}$					2.2		2.6	2.5		2.6	1.9		2.4		4
$(Sr/Nd)_{PM}$					0.2		0.6	0.6		0.8	0.5		2.6		0.3

Sa. no.	Tok 5-3 (Fig. 1a–d)				Tok 6-0						Tok 10-11		Tok 10-19			
Mineral	Wh		Ap		Wh1		Wh2	Ap1		Ap2	Ap		Wh		Ap	
No. anal.	Av. 3	1σ	Av. 6	1σ	Av. 7	1σ	Av. 2	Av. 7	1σ	Av. 4	Av. 3	1σ	Av. 2	1σ	Av. 3	1σ
MgO	3.41	0.04	0.33	0.06	3.45	0.02	3.45	0.37	0.05	0.42	0.91	0.13	3.41	0.01	0.49	0.10
CaO	46.01	0.22	52.73	0.38	44.96	0.65	43.64	51.55	0.81	50.51	50.24	0.56	45.81	0.46	51.45	0.49
Na_2O	2.54	0.03	0.32	0.09	2.66	0.13	2.67	0.27	0.04	0.35	0.90	0.26	1.76	0.19	0.30	0.02
P_2O_5	47.46	0.24	42.39	0.56	46.41	0.55	46.13	42.19	0.57	42.26	41.57	0.55	47.07	0.50	42.34	0.38
Cl	0.01	0.01	1.75	0.32	0.02	0.01	0.01	2.10	0.15	1.42	0.50	0.05	0.03	0.02	2.20	0.48
F	n.d.		n.d.	n.d.	b.d.		b.d.	2.14	0.27	2.95	n.d.	n.d.	n.d.	n.d.	n.d.	n.d.
SrO	0.20	0.03	0.44	0.10	1.43	0.04	2.16	2.68	0.06	3.46	1.60	0.01	1.60	0.09	2.20	0.39
La_2O_3	0.18	0.01	0.18	0.01	0.47	0.07	0.70	0.20	0.05	0.37	0.16	0.00	0.40	0.00	0.13	0.03
Ce_2O_3	0.29	0.02	0.27	0.02	0.73	0.09	1.03	0.29	0.07	0.55	0.28	0.01	0.70	0.02	0.25	0.06
Nd_2O_3	0.08	0.00	0.08	0.01	0.23	0.03	0.33	0.08	0.02	0.17	0.12	0.01	0.27	0.01	0.11	0.03
Total*	100.2	0.3	98.5	0.7	100.4	1.3	100.2	100.5	1.3	100.9	96.3	0.5	101.1	1.1	99.5	1.2
$(La/Nd)_{PM}$	4.2		4.2		3.8		4.1	4.7		4.1	2.5		2.9		2.4	
$(Sr/Nd)_{PM}$	0.2		0.3		0.4		0.4	2.1		1.3	0.9		0.4		1.3	

Sa. no.	8601-17		8530-5b		Mo-104a			Hr-6		St-23		9419-28		Sv-7	
Mineral	Ap (Fig. 4a)		Ap		Ap1		Ap2	Ap		Ap		Ap		Secondary apatite	
No. anal.	Av. 21	1σ	Av. 11	1σ	Av. 6	1σ	Av. 2	Av. 4	1σ	Av. 5	1σ	Av. 10	1σ	Av. 23	1σ
MgO	1.85	0.12	1.24	0.11	1.15	0.09	0.50	0.96	0.16	0.88	0.17	0.67	0.12	0.54	0.18
CaO	49.84	0.67	51.93	0.38	50.71	0.24	50.64	49.79	2.84	52.95	1.00	50.06	1.29	48.09	1.63
Na_2O	0.82	0.11	0.90	0.20	0.85	0.14	0.71	0.15	0.08	0.39	0.14	0.77	0.08	0.01	0.01
P_2O_5	40.91	0.56	41.70	0.54	40.53	0.46	41.07	42.31	0.24	41.17	1.00	41.48	1.35	35.77	1.41
Cl	0.27	0.01	1.11	0.08	2.53	0.11	2.58	1.16	0.25	1.23	0.03	1.68	0.40	0.01	0.01
F	1.16	0.12	0.13	0.12	0.26	0.12	0.35	0.50	0.05	0.79	0.21	0.23	0.23	1.79	0.45
SrO	1.19	0.02	0.63	0.01	1.33	0.01	1.58	0.69	0.04	0.56	0.17	2.33	0.47	1.88	0.23
La_2O_3	0.13	0.01	0.18	0.01	0.30	0.02	0.34	0.08	0.01	0.11	0.03	0.55	0.07	0.01	0.01
Ce_2O_3	0.18	0.01	0.29	0.02	0.45	0.02	0.51	0.10	0.02	0.10	0.02	0.89	0.08	0.07	0.01
Nd_2O_3	0.05	0.00	0.10	0.01	0.15	0.01	0.16	0.05	0.02	0.04	0.01	0.32	0.04	0.01	0.00
Total*	95.8	0.9	97.9	0.6	97.6	0.5	97.7	95.3	2.4	97.6	1.6	98.5	1.9	87.4	2.3
$(La/Nd)_{PM}$	4.4		3.6		3.8		4.0	3.5		5.4		3.3		4.9	
$(Sr/Nd)_{PM}$	1.4		0.4		0.6		0.6	1.0		1.0		0.5		23	

Data from the Montpellier laboratory. Wh, whitlockite; Ap, apatite. Wh2 and Ap2 in Tok xenoliths are relatively coarse anhedral phosphates (≥20 μm wide, Fig. 1e) at grain boundaries of major minerals. N.d., not determined; b.d., below detection limit (~0.1% for F). LA, LA-ICPMS analyses of Durango apatite done at MPI-Chemie, Mainz using NIST-612 reference glass as external standard. $(La/Nd)_{PM}$, $(Sr/Nd)_{PM}$, ratios normalised to primitive mantle [56].

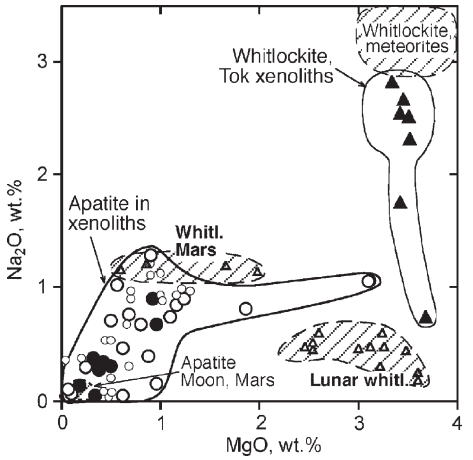

Fig. 5. Na_2O vs. MgO in whitlockite (triangles) and apatite (circles) from terrestrial mantle (filled symbols, Tok xenoliths; empty symbols, other samples; large circles, this study; small circles, data from [9,25–27,33,39]), chondrite and iron meteorites, Martian meteorites, and lunar rocks [11,12,15,16]. Note that the fields of terrestrial apatite and Martian whitlockite overlap.

The Ba–Ti-rich silicate in the Tok xenoliths usually contains ~15% TiO_2 and 10–18% BaO, which is significantly higher than in phlogopites from Tok (2–6% TiO_2; 0.4–4% BaO; Table 1) and other peridotite suites ([9,10], references therein). Some interstitial grains of the same (or related) phase have less Ti and Ba but are very rich in Cr (6–8% Cr_2O_3). The Ba–Ti-rich phase may have higher Ba (and hence look lighter on BSE images; Fig. 4d) in grain cores than in the rims (Table 1). It has very low halogen abundances ($Cl \leq 0.05\%$, $F \leq 0.02$; Table 1). Micas in terrestrial igneous rocks normally have low BaO (<1%, [36]). Ba-rich micas were previously found in pyroxenite xenoliths in volcanic rocks from Pamir [35], like that analysed in this study (Table 1). A biotite with exceptionally high BaO (up to 20%) and TiO_2 (up to 14%) was reported for a nephelinite from Hawaii [40]; this appears to be the only known igneous mica as yet, which has similar abundances of both Ba and Ti to the silicate from Tok. The high Ba and Ti in the mica may be consistent with the substitution scheme [36]:

$$K^+ + 3(Mg, Fe)^{2+} + 3Si^{4+} \leftrightarrow Ba^{2+} + 2Ti^{4+} + 3Al^{3+}$$

The feldspar co-existing with whitlockite and the Ba–Ti-rich silicate is usually rich in alkalis and low in Ca (analysed using a defocused electron beam, 5–10 μm; Table 1). Analyses of feldspar using a focused beam yield lower alkali contents and low totals (89–99%) due to alkali losses [19]. Some EPMA of the feldspar yield appreciable BaO (0.03–0.33%; Table 1) and SrO (0.14%) but these relatively high values may be related to intermittent analytical interferences. Particular care was taken to analyse inclusion-free olivine and spinel in the inferred breakdown products of mica and amphibole (Fig. 4d). Yet, the olivines yield consistently high Al_2O_3 and Cr_2O_3 (0.2–0.4%) while spinels yield high SiO_2 contents (~2%, Table 1). Those chemical features, together with textural evidence, indicate a very rapid breakdown of the parent 'hydrous' phases.

3.3. EPMA for LREE and Sr

Abundances of La, Ce, Nd and Sr were determined by EPMA in apatite and whitlockite from seven Tok xenoliths, the Durango apatite (reference sample) and apatite from seven peridotite xenoliths from southern Siberia and Mongolia (Table 3). The data in this study are not affected by analytical problems responsible for low totals and interferences from adjacent phases in a small number of phosphate analyses reported by [19] using the same method. In particular, apatite (but not whitlockite) commonly breaks down under the electron beam under the conditions required for reliable LREE analyses (25 kV, 30 nA, 60–120 s counting times), apparently because of high volatile contents. In such cases, the analyses were repeated in other spots using either a broader (10 μm) or reduced intensity (10–20 nA) primary beam; appropriate phosphate grains were found by mineral mapping. The Tok phosphates define a tight near-linear La–Ce correlation (Fig. 6a) attesting to high quality of the LREE data.

The phosphates in all Tok xenoliths are rich in LREE (0.1–0.7% La_2O_3); their SrO range from 0.2–0.4% in xenolith 5–3 to 0.8–3.5% in the other samples. These variation ranges are similar to those found in mantle apatite from other xenolith suites (Table 3; [9,10], references therein). Correlations between Sr and LREE are poor or absent (Fig. 6b) apparently because of the contrasted distribution of LREE and Sr between whitlockite, apatite and cpx (see below). The phosphates are strongly enriched in La relative to Nd, their primitive mantle-normalised La/Nd, $(La/Nd)_{PM}$, range from 1.9 to 4.2 (Table 3). $(Sr/Nd)_{PM}$ values are mainly below unity except for three Sr-rich apatites with $(Sr/Nd)_{PM} = 1.3–2.4$. Different abundances of Sr and LREE were found in phosphates with different textural positions in samples 6–0 and 8–31 (Table 3; Fig. 6), i.e. interstitial phosphates (Fig. 1e) may contain twice as much Sr as smaller phosphates in feldspar-rich metasomatic pockets. Vermicular whitlockite intergrown with feldspar in sample 8-40 (Fig. 2a; Electronic Supplement) has more

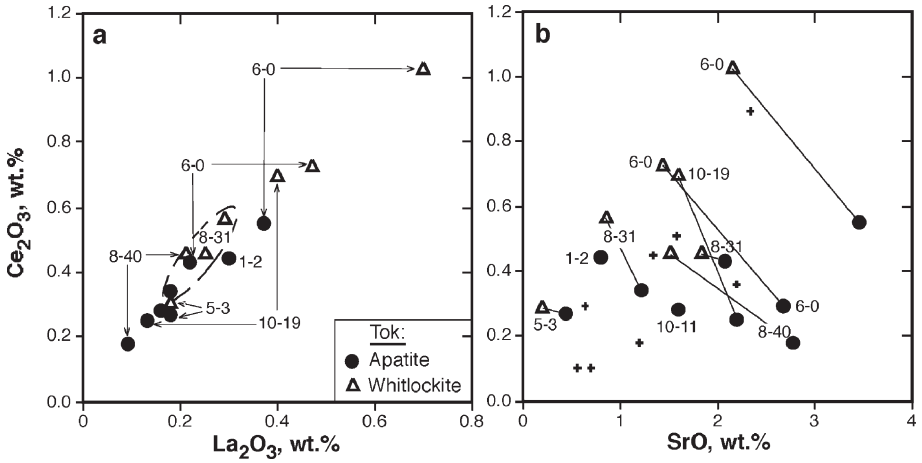

Fig. 6. Ce_2O_3 vs. La_2O_3 (a) and SrO (b) in whitlockite (triangles) and apatite (circles) from Tok xenoliths and apatite (crosses) from xenoliths in central and NE Asian sites (Table 3). Good La–Ce correlation in (a) attests to high quality of the EPMA; whitlockite generally has higher La and Ce and lower Sr than coexisting apatite. No Ce–Sr correlations are seen in (b) for Tok and other apatites indicating that the LREE and Sr are decoupled in the phosphates, e.g. LREE preferentially partition to whitlockite while Sr to apatite; other factors are different Wh/Ap ratios and a more significant share of Sr than REE hosted by coexisting cpx.

SrO than whitlockite intergrown with apatite (2% vs. 1.5%; Table 2).

Whitlockite has systematically higher LREE and lower Sr concentrations than coexisting apatite but the magnitudes of those differences vary greatly from sample to sample and even between different domains in the same sample (Fig. 6). The differences are smallest for sample 5-3 (Fig. 1a–d) and intergranular phosphates in sample 8-31 (Fig. 1e) and greatest (1.5- to 3-fold) for samples 6-0, 8-40 and 10-19. The reasons for those variations are not quite clear. We note that the rare cases when the measured phosphate grains are

Table 4
Trace element abundances (in ppm) in coexisting phosphates and clinopyroxene determined by SIMS and ICPMS

Sa. no.	Tok 8-40 (Fig. 2b, c)											8601-17 Durango	
Mineral	Ap1	Ap2	Wh1	Wh2	Wh/Ap	Cpx	Cpx	WR	Ap/Cpx	Wh/Cpx	Wh-WR (%)	Ap	Ap
Method	SIMS	SIMS	SIMS	SIMS		SIMS	LA	ICPMS				SIMS	LA
Na	1790	2345	11,130	12,950	5.8	14,300	n.d.	846	0.14	0.8	3	5700	n.d.
Sr	19,880	17,430	11,990	12,310	0.7	815	746	92	23	15	23	9490	405
Y	77	74	197	179	2.5	9.70	11.1	1.54	8	19	23	116	393
Zr	1.06	7.3	0.36	0.71	0.1	29.3	30.5	2.5	0.14	0.02	0.0	3.3	0.5
Ba	55.5	37.6	13.6	9.2	0.2	0.37	5.89	10.3	124	30	0.2	2.2	1.2
La	1073	818	1970	1910	2.1	14.4	17.9	6.7	65	134	53	921	2790
Ce	1960	1580	3920	3660	2.1	50.2	54.6	14.5	35	76	49	1456	3380
Pr	202	170	431	395	2.2	8.2	7.6	1.7	23	51	45	150	281
Nd	628	566	1460	1325	2.3	31.7	31.2	6.0	19	44	44	512	870
Sm	66	63	164	151	2.4	5.3	5.0	0.8	12	30	36	68	110
Eu	17.8	13.6	38.3	40.5	2.5	1.70	1.51	0.23	9	23	31	18.4	13.2
Gd	44.8	35.3	123	125	3.1	n.d.	3.38	0.54	12	37	41	52.2	97
Dy	18.0	16.7	40.9	37.1	2.2	1.97	2.24	0.27	9	20	27	25.4	63
Er	7.3	6.8	15.3	14.4	2.1	0.95	0.98	0.11	7	16	26	10.5	33
Yb	7.0	8.2	12.1	9.7	1.4	0.93	0.87	0.08	8	12	26	13.8	25
Th	37.0	28.4	30.8	25.9	0.9	0.11	0.16	0.16	311	269	36	67.5	133
U	20.4	12.3	4.0	1.6	0.2	b.d.	0.05	0.09	0.8	0.1	8	14.1	6.0

B.d., below detection limit; n.d., not determined. The SIMS data for Gd and Yb contain significant corrections for oxide interferences and thus are imprecise. LA, laser ablation ICPMS. LA data for Durango apatite are from this work, those for coarse Cpx are after [19]; both are averages of three analyses. WR, whole-rock analysis by solution ICPMS after [19]. Wh/Ap, Wh/Cp, Ap/Cp, inter-mineral partition coefficients. The share of whitlockite in the WR budget (Wh-WR) was estimated based on P_2O_5 content of 0.16% in the rock [18] and assuming equal amounts of Ap and Wh (0.18 wt.% each).

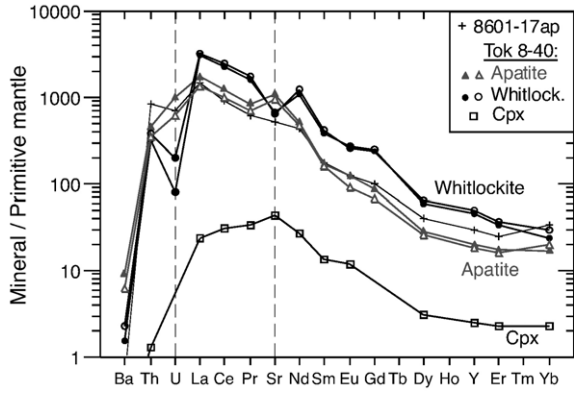

Fig. 7. Primitive mantle-normalised [56] trace element abundances in coexisting whitlockite, apatite and cpx in xenolith 8-40 from Tok. Whitlockite has higher REE and lower Sr and U than apatite. Shown for comparison is apatite in mantle xenolith 8601-17 (Baikal region; Fig. 4a), which has a similar REE pattern, but no Sr anomaly. Note that the SIMS data for Gd and Yb contain significant corrections for oxide interferences and thus are not precise.

clearly in textural equilibrium to each other are their mosaic aggregates in samples 6-0 and 8-40 (Fig. 2c). By contrast, whitlockite may have formed later than apatite in the intergranular phosphate segregations in 8-31 (Fig. 1e).

3.4. SIMS data on trace element abundances in the phosphates

The abundances of trace elements determined by SIMS in coexisting whitlockite, apatite and cpx in Tok xenolith 8-40 (Fig. 2b, c) and in apatite in a veined xenolith from southern Baikal region (Fig. 4a) are given in Table 4. The average abundances of LREE and Sr in apatite and whitlockite obtained by SIMS are close to those from EPMA (Tables 2 and 3). As noted in the preceding section for the EPMA data, the measured whitlockite and phosphate grains in sample 8-40 are both in direct contact and textural equilibrium to each other (Fig. 2c) and hence are most appropriate among samples in this study to constrain equilibrium ap–wh partitioning. Whitlockite contains 1.5–3 times more REE and less Sr, Ba and U than coexisting apatite while Th abundances are similar (Table 4). The trace element pattern of the whitlockite (Fig. 7) has negative anomalies of Sr and U (relative to adjacent REE and Th) while coexisting apatite has a complementary positive Sr anomaly. Apatite 8601-17 (analysed for comparison) has a REE pattern similar to that in apatite 8-40, but shows higher Th/U and no Sr anomaly, consistent with the absence of whitlockite. The abundances of REE, Y, Sr, Th, U in cpx 8-40 are 1-2.5 orders of magnitude lower than in coexisting whitlockite (Fig. 7).

3.5. Trace element signatures of metasomatic cpx coexisting with phosphates

Ionov et al. [19] found that some Tok xenoliths have 2–3 generations of metasomatic cpx with different abundances of sodium and trace elements but they could not establish which (if any) of those cpx generations formed simultaneously with the phosphates. Here, we use BSE images (Fig. 8a) and mineral mapping to show that interstitial apatite and whitlockite in xenoliths 5-3 and 10-19 are intergrown with low-Na (<1% Na_2O) cpx; the latter mantles previously formed cpx with moderate Na_2O contents (~2%) (Fig. 8b). Sample 10-19 also

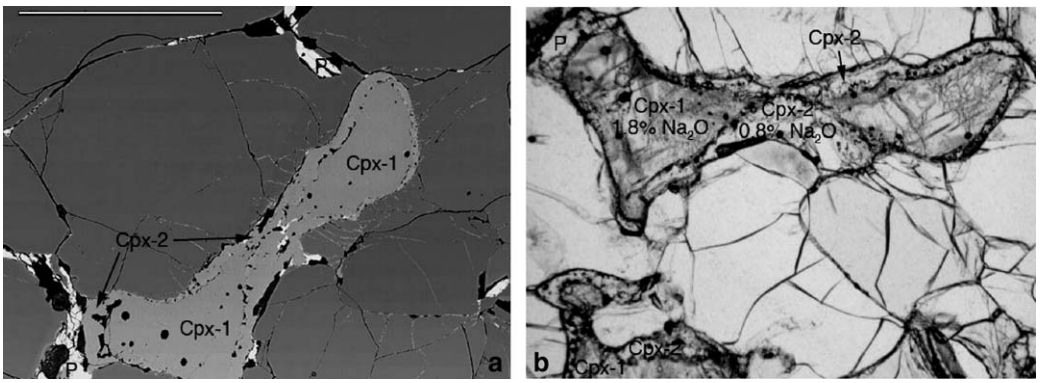

Fig. 8. BSE image (a) and photomicrograph (b) of cpx generations in Tok peridotite xenolith 10-19. White interstitial minerals in (a) are phosphates; they are intergrown (and likely chemically equilibrated) with late-stage, Na-poor cpx-2, which mantles previously formed cpx-1. Average Na_2O contents are indicated for cpx-1 and cpx-2. Trace element patterns for the cpx are shown in Fig. 9. Scale bar, 10 mm.

Table 5
SIMS analyses (in ppm) of different cpx generations in Tok peridotites 5-3 and 10-19

Sa. no.	10–19 cpx						5–3 cpx	
Type	(Na,Cr)-rich		Moderate Na		Low Na		High Na	Low Na
	Av. 2	S.D.%	Av. 4	S.D.%	Av. 4	S.D.%		
Na_2O, %	3.06		1.88		0.77		2.29	0.86
Na	22,730	9	13,930	4	5700	11	17,020	6340
K	14	3	18	1	37	29	8.7	5.6
Sc	90	11	70	5	61	10	55	64
Ti	990	<1	843	4	494	50	503	342
V	319	<1	177	3	166	15	186	217
Cr	14,880	24	6240	15	9220	16	6860	7970
Sr	511	10	535	7	596	13	428	394
Y	15	4	10	6	13	14	5.6	7.4
Zr	122	8	62	3	12	24	34	2.3
La	9.4	11	12.6	6	13.6	15	14.6	10.9
Ce	32	8	39	4	46	19	25.7	26.3
Pr	5.5	8	5.9	4	6.8	17	2.5	3.1
Nd	26	4	27	2	33	14	7.2	10.8
Sm	5.7	6	4.8	7	6.8	10	0.9	1.8
Eu	2.1	15	1.5	10	2.1	13	0.4	0.7
Dy	3.3	10	2.0	5	2.9	17	0.8	1.0
Er	1.4	2	0.91	13	1.1	17	0.5	0.8
Yb	1.3	7	0.88	4	1.0	17	0.7	0.9
Hf	1.8		1.6	6	0.5	42	/0.05/	/0.04/
Th	0.33	<1	0.42	39	0.21	51	0.9	b.d.

B.d., below detection. Hf values in cpx 5-3 are close to detection limits and thus imprecise; yet, they are not much different from Hf=0.024 ppm obtained in cpx 5-3 by LA-ICPMS.

contains a less common Na-rich (~3% Na_2O) cpx, which is not associated with the phosphates. Abundances of trace elements and Na were determined by SIMS in all those cpx generations (Table 5). The low-Na cpx in samples 5-3 and 10-19 has higher abundances of REE and Y (except for La in 5-3) and much lower abundances of Ti and Zr than the cpx with moderate Na_2O contents (Fig. 9). The difference in Zr abundances is striking (5–15-fold). Hf abundances in some cpx are close to detection limits and thus are not precise. The Na-rich cpx 10-19 has higher heavy REE, Ti and Zr and lower LREE abundances than the other two cpx generations (Fig. 9). Thus, the low-Na cpx which formed together with the phosphates has higher LREE

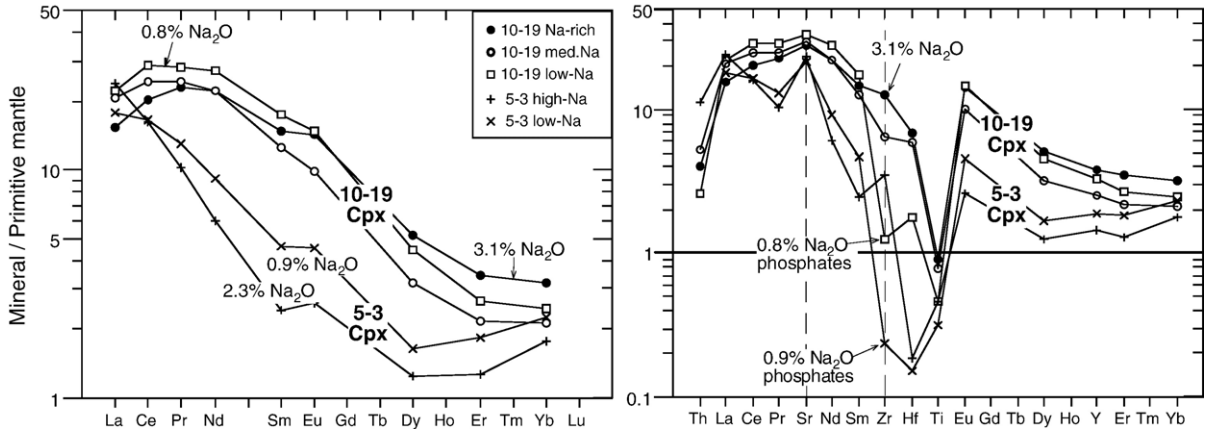

Fig. 9. Primitive mantle-normalised [56] trace element abundance patterns for cpx generations in Tok xenoliths 5-3 and 10-19 (Table 5). Average Na_2O contents are indicated for individual patterns. Note that the low-Na cpx coexisting with phosphates have lowest Zr abundances. The Zr/Hf values in cpx 5-3 seem to vary broadly but they are poorly constrained because Hf abundances are close to detection limits, and only two cpx grains were analysed.

and lower Ti and Zr abundances; this is generally consistent with geochemical features inferred for 'carbonatite' type of metasomatism commonly associated with precipitation of apatite (e.g. [29,39,41,42]). Importantly, Na and LREE are decoupled in the cpx generations, consistent with evidence from whole-rock data [19] for the existence of distinct phosphorus-rich and alkali-rich liquids at late stages of metasomatism.

4. Discussion

4.1. Composition of Tok phosphates vs. extraterrestrial whitlockite and apatite

The contents of major elements in the Tok whitlockite are similar to those in whitlockite from meteorites [11]. By contrast, lunar and Martian whitlockites have much lower Na and Mg contents; Na and Mg in Martian whitlockites overlap the range for apatite in the terrestrial mantle xenoliths (Fig. 5). Lunar and Martian apatites are very low in Na and Mg. Sha [11] argued that lunar whitlockite (<0.5% Na_2O) crystallised originally as β-whitlockite from low-temperature residual melts whereas meteoritic whitlockite, which contains more Na (0.5–3.3% Na_2O), had formed initially as α-whitlockite at higher temperatures and transformed into β-whitlockite upon cooling.

EPMA and SIMS data on REE in whitlockite and apatite from lunar rocks [16] and meteorites [12] show broad variation ranges and in some cases much bigger differences between whitlockite and apatite compositions than in the Tok xenoliths. Neal and Taylor [15] noted that apatite in lunar rocks may form at the latest stages of their solidification, i.e. after crystallisation of 'anhydrous' whitlockite concentrates water and halogens in the last batches of interstitial melts or fluids; hence the two phosphate phases in such rocks may not be coeval. By contrast to the earlier studies on the extraterrestrial samples, we have obtained the first data on whitlockite–apatite partitioning at relatively high temperatures (890–950 °C, [18]) for minerals, which are obviously in textural equilibrium (Fig. 2c). Our results confirm that whitlockite has higher REE than coexisting apatite but they also indicate that whitlockite-to-apatite abundance ratios for REE as high as 10–60 reported for lunar rocks [15] are not likely to be equilibrium features.

4.2. Overlooked whitlockite in the terrestrial mantle?

As shown in Section 3, it is very difficult to distinguish coexisting whitlockite and apatite optically (Figs. 1 and 2). The two phosphates may be intergrown on a μm scale; EPMA of such aggregates with a defocused electron beam (commonly used for volatile-bearing minerals) may yield a range of intermediate compositions (e.g. [19]). Broad chemical variations in terrestrial mantle apatite outlined by earlier work ([9], references therein) and in this paper, together with the possible overlaps between the apatite from the terrestrial mantle and whitlockite from the Moon and Mars (Fig. 5), make it difficult to reliably distinguish apatite from whitlockite in mantle xenolith studies based on EPMA alone. Thus, it is very likely that whitlockite has been overlooked and/or mistakenly identified as apatite in some mantle rocks. For example, an F–Cl-poor phosphate in a mantle xenolith from Kerguelen reported as 'apatite' by Delpech et al. [43] may indeed be whitlockite, e.g. its Na and Mg contents are similar to those of whitlockite from Tok. We also note that direct in situ determination of water in small mineral grains is extremely difficult, and reliable halogen determination by EPMA requires special analytical conditions (e.g. values for fluorine may differ 2-fold depending on the orientation of apatite crystals [44]). Thus, incorrect identification of the phosphate species may contribute to exaggerated estimates of abundances of those volatiles in the terrestrial mantle.

Tok xenoliths 6-0 and 8-40 contain ~0.36 wt.% phosphates based on their whole-rock P_2O_5 (0.16%, [18]). Assuming whitlockite/apatite 1:1 and using SIMS and EPMA mineral and ICPMS whole-rock data from Tables 3 and 4 and [19] it appears that whitlockite accounts for 50–70% of LREE and 20–40% of Y, Sr, Th and heavy to middle REE in the bulk rocks. Thus, whitlockite, even if it coexists with apatite, may be a dominant host for those lithophile trace elements in mantle peridotites, which are strongly enriched in the phosphates relative to cpx ([9], references therein). Its correct identification may be important in constraining the residence of such elements in P_2O_5-rich mantle rocks.

P_2O_5-rich rocks are most common in mainly refractory, strongly metasomatised peridotite suites, like those from Tok. About half of whole-rock analyses of 44 Tok peridotites yielded ≥0.05% P_2O_5; thus they are very likely to contain phosphates [18–20]. We looked for phosphates also in 10 P_2O_5-rich (0.05–0.09%) peridotite xenoliths from nearby southern Siberia and Mongolia using EPMA mapping and found apatite (but no whitlockite) in all of them (Tables 2 and 3); previously apatite was found by optical microscopy and routine EPMA only in two of those samples. Phosphates sufficiently large for EPMA might

occur also in peridotites with lower P_2O_5 (e.g. 0.02–0.05%), which are much more common, as well as in veined xenoliths. We believe that whitlockite can most likely be found in xenoliths affected by the "feldspar-Ti-oxide" mantle metasomatism attributed to water-poor melts or fluids [31]. Such xenoliths are ubiquitous in the Russian far east (e.g. Tok) and have also been reported from Kerguelen [31,32,34,43]. Unfortunately, none of the 10 xenoliths, in which we looked for the phosphates, shows such metasomatism.

A particular find was made in xenoliths from Sveyaga (Sikhote-Alin, Russian far east). EPMA mapping of five P_2O_5-rich ($\geq$0.08%) peridotites from that site found only secondary (post-eruption) apatite, which forms massive cross-cutting and interstitial veins and pockets. This apatite is distinct from all mantle-derived phosphates in this study by very low totals (<90%) and low concentrations of Na, Cl and La ($\leq$0.02%; Sv-7 in Table 3). Care should be taken not to confuse such late-stage materials with mantle-derived, metasomatic phosphates.

4.3. 'Dry' metasomatic fluids in the terrestrial mantle

The whitlockite-bearing metasomatic aggregates typically contain empty vugs (Figs. 1 and 2) and hence may have crystallised from fluid-rich liquids. It appears that crystallization of those hypothetical liquids produced residual fluids that initially filled the cavities and later escaped. The whitlockite is a water- and halogen-free phosphate. Moreover, the whitlockite-bearing peridotites do not contain 'hydrous' silicate phases and hence the hypothetical fluid is inferred to have been poor in water because hydrous fluids react with host peridotites to produce amphibole or phlogopite (e.g. [2,45,46]). We infer from the textural and chemical evidence that melts or fluids, which precipitated whitlockite (with or without apatite) had lower activities of water and halogens than fluids that only precipitated apatite. This inference is further supported by evidence for breakdown of volatile-bearing mica and amphibole documented in the Tok xenoliths containing whitlockite. The Ba–Ti-rich mineral in the latter xenoliths is low in halogens and may be poor in water based on its Raman spectra; its modal abundances are negligible anyway (Fig. 4b). Thus, reaction of the hypothetical 'dry' fluids with pre-existing 'hydrous' minerals produced 'dry' assemblages, with alkalis mainly hosted by alkali feldspar instead of mica and amphibole.

The origin of such fluids is enigmatic, mainly because water and halogens are highly mobile, 'incompatible' mantle components and thus are expected to strongly concentrate in melts and fluids relative to solid residues [47]. Hence, the tenet of mantle petrology that low-degree mantle-derived fluids are likely to have high water and halogen contents does not appear to apply to the upper mantle domain beneath Tok and possibly elsewhere (e.g. Kerguelen, [43]). We speculate that essentially water-free mantle fluids may consist mainly of CO_2 or alkaline silicate melts rich in CO_2 and phosphates. Liquid carbonates could be another potentially significant component in such liquids, however no carbonates have been found in any Tok xenolith in this or earlier [18–20] studies. The hypothetical dry fluids may form by one of the following scenarios: (1) from dry mantle domains; (2) as residual products of interaction of water-bearing fluids with alkali-rich mantle wall rocks, such that all initially present water is bound by precipitation of metasomatic mica and amphibole; (3) by immiscibility from complex silicate–carbonate liquids [48,49] if water and halogens fractionate mainly into the silicate liquids to yield a 'dry' carbonate fluid.

Partial melting of the upper mantle involving such fluids or whitlockite-bearing rocks may yield basaltic liquids with peculiar geochemical characteristics. Importantly, such liquids may have low water and halogen abundances in combination with high P_2O_5 (e.g. [50]) as well as unusual Th/U, Sr/Nd.

4.4. Late-stage origin of whitlockite in the Tok mantle?

Textural, chemical and isotope data on the Tok xenolith suite [18,19,21] indicate that it experienced a complex sequence of metasomatic events. Whitlockite likely formed during the latest of those events, i.e. only shortly before the xenoliths were brought up to the surface. One of the arguments for this is that whitlockite commonly coexists with a specific (low-Na) cpx generation chemically distinct from other cpx in the same samples. The apparent lack of chemical equilibrium between those cpx generations could not have survived for a long time at high ambient T (890–950 °C) in the mantle after the formation of cpx associated with whitlockite. Ionov et al. [19] inferred that metasomatic peridotites enriched in phosphorus, alkalis and volatiles were initially formed in the shallow Tok mantle by an ancient, large-scale enrichment event followed by a period of thermal relaxation. In some of those rocks, amphibole and mica may have originally coexisted with apatite, like in other metasomatic xenoliths worldwide [9,25–27,29,51]. By contrast, whitlockite in the Tok xenoliths never coexists with amphibole or phlogopite

but is commonly associated with their breakdown products. This is possible if whitlockite formed in the most recent metasomatic episode due to infiltration of 'anhydrous' fluids. Those fluids may not necessarily have been rich in phosphorus. They could probably react with pre-existing 'hydrous' apatite to cause its partial or complete transformation into whitlockite (simultaneously with the breakdown of phlogopite and amphibole). Some xenoliths indeed show textural evidence for a late-stage origin of whitlockite (Fig. 1e); variable ap/wh ratios for REE and Sr in Tok xenoliths may be related to a lack of equilibrium between the two phosphates consistent with such a process. In many cases, however, apatite and whitlockite appear to be in local textural equilibrium (Fig. 2c), which may be possible if the inferred recent metasomatic episode was sufficiently long-living to enable local re-crystallization of the pre-existing metasomatic assemblages.

4.5. Dry fluids and mantle rheology

The differences in volatile abundances are believed to be a major reason why the global tectonics of the Earth and the composition of its crust are different from those of Mars and the Moon. Even small amounts of water may significantly affect mantle rheology and seismic properties [5,52]. As little as several hundred parts per million of water present in the Earth's mantle may decrease its melting point by 100–200 °C and significantly increase its sodium abundances [53,54] while larger amounts of water also shift compositions of partial melting products from basaltic to andesitic and thus play a fundamental role in producing continental crust [1] and driving plate tectonics. The presence of water and halogens in mantle-derived melts and fluids strongly affects the oxygen fugacity and solubility of certain trace elements and is relevant to their concentration and creation of magmatic ore deposits [55]. We conclude that parts of the Earth's deep interior are nearly as dry as those of smaller solar system bodies, and hence some petrogenetic processes in the Earth's interior may resemble those in the Moon and Mars much more than currently assumed.

5. Summary

We report the discovery of the anhydrous and halogen-free phosphate mineral whitlockite in terrestrial mantle rocks and argue that portions of the Earth's deep interior may be nearly as 'dry' as those of the Moon, Mars and parental bodies of meteorites (where whitlockite is common), even if mantle rocks are theoretically capable to accommodate water under high pressures.

Whitlockite may be an important host for LREE, Sr, Y, Th, U in parts of the upper mantle. Its presence in the source regions of mantle-derived magmas may affect the abundances of the lithophile elements as well as of halogens and water, and eventually Sr–Nd–Pb isotope signatures (assuming long-term closed-system evolution of the source regions), in the partial melting products erupted on the Earth's surface.

Acknowledgements

DAI thanks A. El Goresi for advice, J.-L. Bodinier for support at Université Montpellier 2 (France), G. Brey for support at Goethe-Universitaet (Frankfurt, Germany), B. Stoll, N. Groschopf, D. Kuzmin and H. Höfer for analytical assistance. Andreas Möller generously provided the Durango apatite standard. EPMA at Mainz were obtained with support from W. Paul award (Humboldt Foundation, Germany) to A.V. Sobolev. We appreciate reviews by two anonymous reviewers and editorial handling by R. Carlson.

Appendix A. Supplementary data

Supplementary data associated with this article can be found, in the online version, at doi:10.1016/j.epsl.2006.02.012.

References

[1] P.E. van Keken, The structure and dynamics of the mantle wedge, Earth Planet. Sci. Lett. 215 (2003) 323–338.
[2] M. Olafsson, D.H. Eggler, Phase relations of amphibole, amphibole-carbonate, and phlogopite-carbonate peridotite: petrologic constraints on the asthenosphere, Earth Planet. Sci. Lett. 64 (1983) 305–315.
[3] H. Iwamori, Transportation of H_2O and melting in subduction zones, Earth Planet. Sci. Lett. 160 (1998) 65–80.
[4] J.F. Forneris, J.R. Holloway, Phase equilibria in subducting basaltic crust: implications for H_2O release from the slab, Earth Planet. Sci. Lett. 214 (2003) 187–201.
[5] R.W. Luth, Mantle volatiles—distribution and consequences, in: R.W. Carlson (Ed.), Treatise on Geochemistry, The Mantle and Core, vol. 2, Elsevier, Amsterdam, 2003, pp. 319–362.
[6] N. Bolfan-Casanova, H. Keppler, D.C. Rubie, Water partitioning between nominally anhydrous minerals in the $MgO–SiO_2–H_2O$ system up to 24 GPa: implications for the distribution of water in the Earth's mantle, Earth Planet. Sci. Lett. 182 (2000) 209–221.
[7] D. Bercovici, S.-I. Karato, Whole-mantle convection and the transition-zone water filter, Nature 425 (2003) 39–44.
[8] M.A. Menzies, C.J. Hawkesworth (Eds.), Mantle Metasomatism, Academic Press, London, 1987, p. 500.

[9] D.A. Ionov, S.Y. O'Reilly, W.L. Griffin, Volatile-bearing minerals and lithophile trace elements in the upper mantle, Chem. Geol. 141 (1997) 153–184.
[10] D.G. Pearson, D. Canil, S.B. Shirey, Mantle samples included in volcanic rocks: xenoliths and diamonds, in: R.W. Carlson (Ed.), Treatise on Geochemistry, The Mantle and Core, vol. 2, Elsevier, 2003, pp. 171–276.
[11] L.-K. Sha, Whitlockite solubility in silicate melts: some insights into lunar and planetary evolution, Geochim. Cosmochim. Acta 64 (2000) 3217–3236.
[12] W. Hsu, Rare earth element geochemistry and petrogenesis of miles (IIE) silicate inclusions, Geochim. Cosmochim. Acta 67 (2003) 4807–4821.
[13] M. Anand, L.A. Taylor, C.R. Neal, G.A. Snyder, A. Patchen, Y. Sano, K. Terada, Petrogenesis of lunar meteorite EET 96008, Geochim. Cosmochim. Acta 67 (2003) 3499–3518.
[14] B.L. Jolliff, L.A. Haskin, R.O. Colson, M. Wadhwa, Partitioning in REE-saturating minerals: theory, experiment, and modelling of whitlockite, apatite, and evolution of lunar residual magmas, Geochim. Cosmochim. Acta 57 (1993) 4069–4094.
[15] C.R. Neal, L.A. Taylor, Evidence for metasomatism of the lunar highlands and the origin of whitlockite, Geochim. Cosmochim. Acta 55 (1991) 2965–2980.
[16] A.L. Albee, A.A. Chodos, Microprobe investigations of Apollo 11 samples, Proc. Apollo 11 Lunar Sci. Conf. (1970) 135–157.
[17] D.A. Ionov, A.W. Hofmann, A. Gurenko, E. Hellebrand, G. Montagnac, P. Gillet, Whitlockite and (Ba,Ti)-rich mica in Siberian xenoliths indicate 'dry' conditions in parts of terrestrial mantle, Geochim. Cosmochim. Acta 69 (2005) (Abstract EGU05-A-03535).
[18] D.A. Ionov, V.S. Prikhodko, J.-L. Bodinier, A.V. Sobolev, D. Weis, Lithospheric mantle beneath the south-eastern Siberian craton: petrology of peridotite xenoliths in basalts from the Tokinsky Stanovik, Contrib. Mineral. Petrol. 149 (2005) 647–665.
[19] D.A. Ionov, G. Chazot, C. Chauvel, C. Merlet, J.-L. Bodinier, Trace element distribution in peridotite xenoliths from Tok, SE Siberian craton: a record of pervasive, multi-stage metasomatism in shallow refractory mantle, Geochim. Cosmochim. Acta 70 (2006) 1231–1260.
[20] D.A. Ionov, I. Chanefo, J.-L. Bodinier, Origin of Fe-rich lherzolites and wehrlites from Tok, SE Siberia by reactive melt percolation in refractory mantle peridotites, Contrib. Mineral. Petrol. 150 (2005) 335–353.
[21] D.A. Ionov, S.B. Shirey, D. Weis, G. Brügmann, Os–Hf–Sr–Nd isotope and PGE systematics of spinel peridotite xenoliths from Tok, SE Siberian craton: effects of pervasive metasomatism in shallow refractory mantle, Earth Planet. Sci. Lett. 241 (2006) 47–64.
[22] Handbook of Minerals Raman spectra. Free database 2003, Laboratoire de Sciences de la Terre, ENS-Lyon, France, 2000–2005.
[23] E. Jarosewich, J.A. Nelen, J. Norberg, Reference samples for electron microprobe analysis, Geostand. Newsl. 4 (1980) 43–47.
[24] E. Hellebrand, J.E. Snow, P. Hoppe, A.W. Hofmann, Garnet-field melting and late-stage refertilization in 'residual' abyssal peridotites from the Central Indian Ridge, J. Petrol. 43 (2002) 2305–2338.
[25] F.A. Frey, D.H. Green, The mineralogy, geochemistry and origin of lherzolite inclusions in Victorian basanites, Geochim. Cosmochim. Acta 38 (1974) 1023–1059.
[26] S.Y. O'Reilly, W.L. Griffin, Mantle metasomatism beneath Victoria, Australia: I. Metasomatic processes in Cr-diopside lherzolites, Geochim. Cosmochim. Acta 52 (1988) 433–447.
[27] G. Chazot, M. Menzies, B. Harte, Determination of partition coefficients between apatite, clinopyroxene, amphibole, and melt in natural spinel lherzolites from Yemen: implications for wet melting of the lithospheric mantle, Geochim. Cosmochim. Acta 60 (1996) 423–437.
[28] J.-L. Bodinier, M.A. Menzies, N. Shimizu, F.A. Frey, E. McPherson, Silicate, hydrous and carbonate metasomatism at Lherz, France: contemporaneous derivatives of silicate melt-harzburgite reaction, J. Petrol. 45 (2004) 299–320.
[29] G. Rivalenti, A. Zanetti, M. Mazzucchelli, R. Vannucci, C.A. Cingolani, Equivocal carbonatite markers in the mantle xenoliths of the Patagonia backarc: the Gobernador Gregores case (Santa Cruz Province, Argentina), Contrib. Mineral. Petrol. 147 (2004) 647–670.
[30] D.A. Ionov, S.Y. O'Reilly, I.V. Ashchepkov, Feldspar-bearing lherzolite xenoliths in alkali basalts from Hamar-Daban, southern Baikal region, Russia, Contrib. Mineral. Petrol. 122 (1995) 174–190.
[31] D.A. Ionov, M. Grégoire, V.S. Prikhod'ko, Feldspar-Ti-oxide metasomatism in off-cratonic continental and oceanic upper mantle, Earth Planet. Sci. Lett. 165 (1999) 37–44.
[32] F. Kalfoun, D. Ionov, C. Merlet, HFSE residence and Nb–Ta ratios in metasomatised, rutile-bearing mantle peridotites, Earth Planet. Sci. Lett. 199 (2002) 49–65.
[33] F. Chalot-Prat, M. Arnold, Immiscibility between calciocarbonatitic and silicate melts and related wall rock reactions in the upper mantle: a natural case study from Romanian mantle xenoliths, Lithos 46 (1999) 627–659.
[34] M. Grégoire, J.-P. Lorand, S.Y. O'Reilly, J.-Y. Cottin, Armalcolite-bearing, Ti-rich metasomatic assemblages in harzburgite xenoliths from the Kerguelen Islands: implications for the oceanic mantle budget of high-field strength elements, Geochim. Cosmochim. Acta 64 (2000) 673–694.
[35] V.S. Lutkov, Evidence for mantle metasomatism from micas in the alkali basalts of the southern Tien Shun, Tajikistan, Petrology 6 (1998) 47–61.
[36] S.W. Bailey (Ed.), Micas. Reviews in Mineralogy, vol. 13, Miner. Soc. Amer., Washington, DC, 1984, p. 584.
[37] S. Press, G. Witt, H.A. Seck, D.A. Ionov, V.I. Kovalenko, Spinel peridotite xenoliths from the Tariat Depression, Mongolia: I. Major element chemistry and mineralogy of a primitive mantle xenolith suite, Geochim. Cosmochim. Acta 50 (1986) 2587–2599.
[38] D.A. Ionov, Spinel peridotite xenoliths from the Shavaryn-Tsaram volcano, northern Mongolia: petrography, major element chemistry and mineralogy, Geol. Carpath. 37 (1986) 681–692.
[39] E.H. Hauri, N. Shimizu, J.J. Dieu, S.R. Hart, Evidence for hotspot-related carbonatite metasomatism in the oceanic upper mantle, Nature 365 (1993) 221–227.
[40] W.L. Manske, R.C. Ewing, K. Keil, Barian–titanian biotites in nephelinites from Oahu, Hawaii, Am. Mineral. (1979) 156–159.
[41] R.L. Rudnick, W.F. McDonough, B.C. Chappell, Carbonatite metasomatism in the northern Tanzanian mantle, Earth Planet. Sci. Lett. 114 (1993) 463–475.
[42] D.A. Ionov, J.-L. Bodinier, S.B. Mukasa, A. Zanetti, Mechanisms and sources of mantle metasomatism: major and trace element compositions of peridotite xenoliths from Spitsbergen in the context of numerical modeling, J. Petrol. 43 (2002) 2219–2259.

[43] G. Delpech, M. Gregoire, S.Y. O'Reilly, J.Y. Cottin, B. Moine, G. Michon, A. Giret, Feldspar from carbonate-rich silicate metasomatism in the shallow oceanic mantle under Kerguelen Islands (South Indian Ocean), Lithos 75 (2004) 209–237.
[44] M.L. Kohn, J. Rakovan, J.M. Hughes (Eds.), Phosphates: Geochemical, Geobiological, and Materials Importance, Mineral. Soc. Amer., 2003, 742 pp.
[45] P.J. Wyllie, Mantle fluid compositions buffered in peridotite–CO_2–H_2O by carbonates, amphibole, and phlogopite, J. Geol. 86 (1978) 687–713.
[46] K. Niida, D.H. Green, Stability and chemical composition of pargasitic amphibole in MORB pyrolite under upper mantle conditions, Contrib. Mineral. Petrol. 135 (1999) 18–40.
[47] P.J. Michael, The concentration, behavior and storage of H_2O in the suboceanic upper mantle: implications for mantle metasomatism, Geochim. Cosmochim. Acta 52 (1988) 555–566.
[48] W.-j. Lee, P.J. Wyllie, Processes of crustal carbonatite formation by liquid immiscibility and differentiation, elucidated by model systems, J. Petrol. 39 (1998) 2005–2013.
[49] M.B. Kamenetsky, A.V. Sobolev, V.S. Kamenetsky, R. Maas, L. V. Danyushevsky, R. Thomas, N.P. Pokhilenko, N.V. Sobolev, Kimberlite melts rich in alkali chlorides and carbonates: a potent metasomatic agent in the mantle, Geology 32 (2004) 845–848.
[50] J.V. Smith, J.S. Delaney, R.L. Hervig, J.B. Dawson, Storage of F and Cl in the upper mantle: geochemical implications, Lithos 14 (1981) 133–147.
[51] D.A. Ionov, S.Y. O'Reilly, M.G. Kopylova, Y.S. Genshaft, Carbonate-bearing mantle peridotite xenoliths from Spitsbergen: phase relationships, mineral compositions and trace element residence, Contrib. Mineral. Petrol. 125 (1996) 375–392.
[52] T. Mizukami, S.R. Wallis, J. Yamamoto, Natural examples of olivine lattice preferred orientation patterns with a flow-normal a-axis maximum, Nature 427 (2004) 432–436.
[53] P.D. Asimow, C.H. Langmuir, The importance of water to oceanic mantle melting regimes, Nature 421 (2003) 815–820.
[54] M. Ligi, E. Bonatti, A. Cipriani, L. Ottolini, Water-rich basalts at mid-ocean-ridge cold spots, Nature 434 (2005) 66–69.
[55] W. Sun, R.J. Arculus, V.S. Kamenetsky, R.A. Binns, Release of gold-bearing fluids in convergent margin magmas prompted by magnetite crystallization, Nature 431 (2004) 975–978.
[56] A.W. Hofmann, Chemical differentiation of the Earth: the relationship between mantle, continental crust, and oceanic crust, Earth Planet. Sci. Lett. 90 (1988) 297–314.